



Pixel Detector Mechanics Conceptual Design Review

ATLAS Project Document No:

ATL-IP-ES-0025

Institute Document No.

Created: **25/06/2001**

Page: **1 of 2**

Modified:

Rev. No.: **1**

Technical Specification

Pixel Detector Disk Support Rings

Abstract

This document describes the technical specifications for the design and fabrication of the disk support rings for the ATLAS pixel detector.

Prepared by:

M. Gilchriese, W. Miller

Checked by:

Approved by:

Distribution List

History of Changes

<i>Rev. No.</i>	<i>Date</i>	<i>Pages</i>	<i>Description of changes</i>

Table of Contents

1	INTRODUCTION	4
2	DIMENSIONS AND ENVELOPES.....	4
3	INTERFACES.....	4
3.1	Disk Sectors.....	4
3.2	Global Support Frame	5
3.3	Services.....	6
4	FINAL ASSEMBLY	6
5	SURVEY REQUIREMENTS	6
6	LOAD CONDITIONS, STABILITY AND ANALYSIS.....	6
7	OTHER REQUIREMENTS	6
8	MATERIALS.....	7
9	QUALIFICATION TESTS	7
9.1	Materials	7
9.2	As-built Dimensions	7
9.3	Load Tests	7
9.4	Sector Mounting Test.....	7
10	QUALITY ASSURANCE.....	7
11	REFERENCES.....	7

1 Introduction

The disk support rings for the ATLAS detector support the disk sector local supports and are held by the global support frame of the pixel detector as shown in Figure 1. There are six disk support rings in the



Figure 1. ATLAS Pixel disk structures (support rings and disk sectors) inside the global support frame.

complete Pixel Detector. All six disks are identical.

Two prototype rings have been fabricated and loaded with prototype disk sectors. These prototypes corresponded to a larger radius for the pixel detector but the analysis and test results (particularly of the 2nd prototype) are applicable to the current design. Analysis of the second prototype is described in ref. 1. Test results are described in ref. 2.

2 Dimensions and Envelopes

The current baseline dimensions of the disk support ring are shown in Figure 2. Detailed envelopes will be addressed later in the creation of fabrication drawings for the rings and subcomponents of the rings. The current envelopes for the radial dimensions of the ring exceed the nominal by 0.1 mm. The envelope for the thickness (including bow) is 0.2mm (each side) greater than the nominal dimensions.

There are 24 sector support buttons on each ring, arranged in groups of three for each sector. The surfaces of the buttons (averaged over the button) in a group of three are to be in a plane with a tolerance of ± 0.1 mm. Similarly the surface of any button with respect to the average of all buttons should not deviate from the average by more than ± 0.1 mm.

3 Interfaces

The principal interfaces to the disk support ring are (1) the disk sectors; (2) the global support frame; and (3) services (cables) from the modules mounted on the disk sectors.

3.1 Disk Sectors

The disk sectors are mounted on the disk support rings by fasteners that precisely align the sectors to the three mounting points on the ring. The locations of the three mounting points are to be set by tooling referenced to a master gauge used to fabricate the sectors. The aim is to allow any sector to be mounted

on any ring at any point on the ring. The nominal spacing between the ring facing and the sector facing is 2.75 mm and the minimum spacing is 2.5 mm.

There must be no uncontrolled electrical connection between the disk sector and the support ring. This is currently implemented by having non-conducting buttons on the disk sectors.

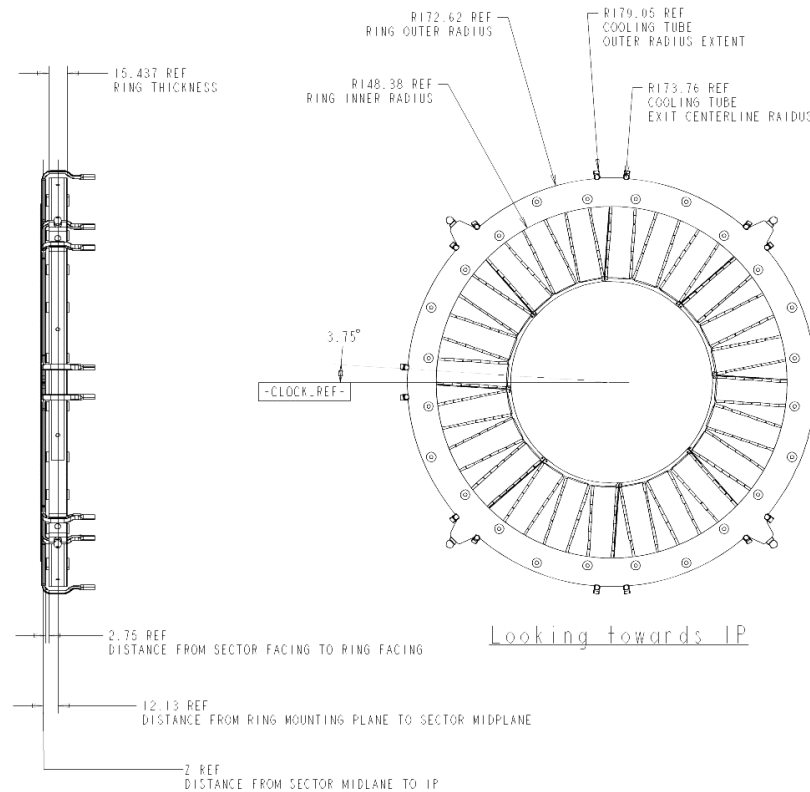


Figure 2. Current baseline dimensions of the disk support ring.

3.2 Global Support Frame

The disk support rings are held by four mounts in the global support frame. The mounting concept is illustrated in Figure 3.

These mounts have limited adjustment to allow the support ring to be centered on the axis of the frame, as well as provide means for disk removal. The small amount of travel that is provided by a built in differential lead screw, retracts the conical ball seat away from disk support ring spherical ball mount. An external access to this screw mechanism is provided. All four mounts use a precision spherical ball and conical seat combination to rigidly fix the contact points in XYZ. Rotation about the local contact point is permitted to limit moment transfer from the Global Support frame.



Figure 3. PEEK based adjustable radial mount for the disk support ring. View rotated 45° for convenience of display.

There must be no uncontrolled electrical connection between the disk ring and the global support. This is currently accomplished by having a non-conducting bushing in the global support frame.

3.3 Services

Electrical services(pigtails) pass over the support ring. Strain relief, if required, will be provided by gluing supports on to the support ring. The design of the strain relief has not been done but all strain relief elements will be added by LBNL after fabrication of a ring is complete. Fabrication and mounting of the strain relief pieces is not a responsibility of the ring fabrication vendor.

4 Final Assembly

Tooling is used to hold and locate the ring for assembly into the global support. The sector mounting holes are used to hold and align the ring to the tooling. No additional holes are required.

5 Survey Requirements

The location of modules on one side of the disk sectors are to be referenced by an optical coordinate measuring machine to the survey targets on the ring. These targets will be used to locate the ring inside the global support frame. These targets are not defined at this time but the location is to be on the four "ears" on the ring so that they are visible with sectors mounted on the ring. The ring survey targets are located on the side of the ring away from the IP. The targets for survey of the disks after mounting in the global support frame are not yet defined.

6 Load Conditions, Stability and Analysis

Finite element and other analyses are to be done on the ring. The critical requirements are that deflections under gravity, imposed loads, vibrations(stability) or as the result of cool down from room temperature. We calculate the allowable values assuming a 20% or less degradation in the pixel resolution and furthermore assume this is apportioned among the disk sector, disk support ring and global support in the ratio 1:2:4, respectively. Tolerance values are assumed to be (rms value) $\times \sqrt{12}$. With these assumptions, the tolerance(rms) requirements in ϕ , R and Z, are 12(3.4), 100(29), 212(62) microns, respectively. Analysis of the current design is described in ref. 3.

7 Other Requirements

The ring will be coated with Parylene(0.008-0.012 mm thick) after fabrication to contain conducting carbon dust or fragments.

8 Materials

The ring faceplates are to be carbon-carbon (C-C) material identical to the material used for sector fabrication. The nominal thickness of this material is 0.44mm. C-Channels, outer and inner, are used to bond the two C-C faces together. Woven cloth material (YSH50 graphite fiber), impregnated with cyanate ester resin is used for constructing the C-Channels. A 0/45/-45/0 fiber orientation is used for laying up the woven cloth, resulting in a nominal wall thickness of 0.5mm. The 24 inserts for mounting the sectors are machined and bonded to the front and back surfaces of the faceplates. Two insert materials have been identified for this application, PEEK and 3D C-C. The 3D C-C is preferred from a thermal dimensional stability standpoint. Material for supporting the 4 spherical mounting balls on the ring is 3D C-C. Hysol 9396 room temperature curing adhesive is used in all the bonding steps for joining this assembly. With the exception of the precision spherical ball on the disk ring, all mount materials are PEEK (thermoplastic). The spherical balls will most likely be from a ceramic material, although aluminum is an option.

9 Qualification Tests

Qualifications tests are to be performed by the fabrication vendor on materials to be used in the ring construction and on each ring after fabrication. LBNL will also perform qualification tests.

9.1 Materials

Tensile modulus and strength tests are to be done on the carbon-carbon material used for the faceplates and on the material used for the C-channels in the ring construction.

9.2 As-built Dimensions

The fabrication vendor will measure the average thickness, inner and outer radius of each ring. The critical dimensions of each ring(location of sector mounting holes and mounting points, planarity of the mounting buttons) are to be measured by LBNL for each ring.

9.3 Load Tests

The deflection of the ring midway between each of the support points is to be measured up to a 10N load by LBNL.

9.4 Sector Mounting Test

LBNL will provide a few test sectors and mounting pins/bolts to the fabrication vendor. The fabrication vendor will demonstrate that a test sector can be mounted at any location on all rings.

10 Quality Assurance

The fabrication vendor will provide a quality control plan to LBNL as part of the fabrication contract.

11 References

1. *Thermoelastic Static and Modal Analysis Of Composite Support Ring for a Pixel Detector Planar Array, HTN-106020-0001, June 1,2000*
2. *Static and Modal Testing of Composite Support Ring for a Pixel Detector Planar Array, HTN-106020-0002, June 1, 2000*
3. *Analysis of ATLAS Disk Support Ring, 432mm Global Support Structure, HTN-106210-0001, April 22, 2001*

Thermoelastic Static and Modal Analysis Of Composite Support Ring for a Pixel Detector Planar Array

W.O. Miller
HYTEC, Inc.
June 1, 2000

Abstract

Thermal and gravity induced strains, and natural modes of vibration are calculated for a mounting ring that will be used in testing a pixel detector thermostructure concept for the ATLAS Pixel Detector. Development of the thermostructure is supported by a Department of Energy Phase II SBIR. The mounting ring is hollow, consisting of carbon-carbon (C-C) face sheets separated by PEEK posts and edge closeouts constructed from a resin based composite material. The ring is supported at three points around its perimeter. The design aspect of the three attachment connections is part of this study.

TABLE OF CONTENTS

1. INTRODUCTION.....	3
2. DISCUSSION OF ANALYTICAL RESULTS	4
2.1 FEA ANALYSIS OF SUPPORT RING	5
2.1.1 <i>Support Ring Static Analysis.....</i>	<i>5</i>
2.1.2 <i>Support Ring (Only) Mode Shapes and Frequencies.....</i>	<i>9</i>
2.2 FEA OF DISK ASSEMBLY.....	10
2.2.1 <i>Disk Assembly Mode Shapes and Frequencies.....</i>	<i>10</i>
2.2.2 <i>Disk Assembly Static FEA.....</i>	<i>15</i>
3. SUMMARY AND RECOMMENDATIONS FOR FUTURE WORK.....	18
4. REFERENCES.....	19

1. Introduction

The primary objective of the “*Ultra-Lightweight Carbon-Carbon Cooling Structure for Pixel and Silicon Strip Detectors*” Phase 2 SBIR is to develop an ultra-lightweight, highly stable structure for supporting and cooling a flat panel array of pixel modules. The structure, entitled *thermostructure* is being proposed by HYTEC for use in the ATLAS Detector, one of two detectors scheduled for the Large Hadron Collider experiment. As part of the SBIR, HYTEC is to design and test a composite ring for supporting the thermal structures (sectors) in a disk-like arrangement. The ring is to accommodate an array of 12-sectors at nominally a 199.5 mm radius. This technical note discusses the finite element analyses performed to explore the ring structural design characteristics, and to provide data for comparison with the experimental results.

The composite ring is a box-like structure composed of a front and back carbon-carbon facing bonded together with C-Channels located on the inner and outer ring periphery. A 3D model of the ring is shown in Fig. 1.

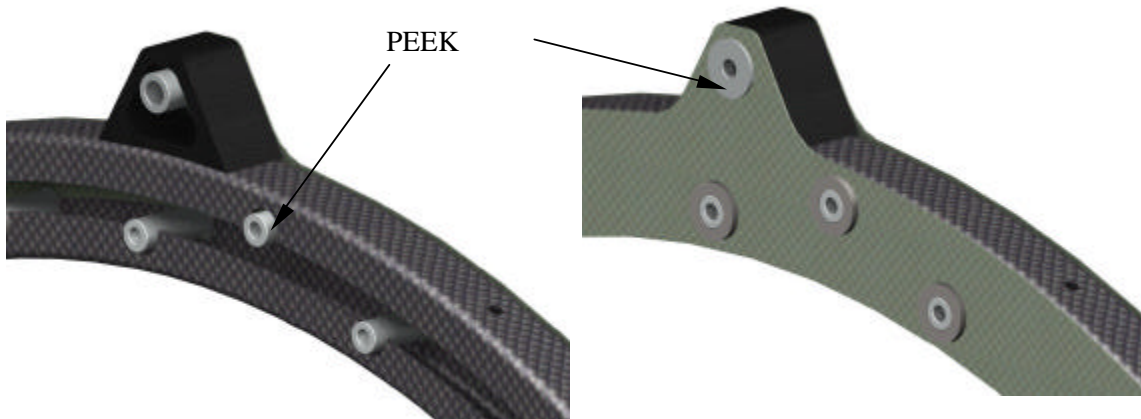


Figure 1: Left inset is an illustration of the inner and outer C-Channels for the composite ring, front facing removed. Right inset depicts the back facing installed and the bonding of the PEEK washers to the back face.

The ring and 12 sectors comprise a disk assembly. This assembly is supported at three points on its periphery. Fig. 2 is a view of the assembly with the 12-sectors removed. The support points in the lower two quadrants support the gravitational load imposed on the disk. The upper support point, in its final configuration, will provide rotational restraint about an axis normal to the ring (Z). All three points restrain the ring in a direction normal to the ring (Z).

The final structural design of the ring is influenced to a significant extent by the method used to mount the disk assembly in the pixel detector outer frame. Although, the design of the mounts (a local support issue) is not part of this SBIR effort, it is important that this element be considered in the design of the ring. As a first step, the support boundary conditions chosen for the ring will emulate only the reaction at the ring and the mount interface. In the final analysis, the compliance in the mount and the support frame

must be included in any structural representation of the pixel disk assembly. The complete model is needed to verify the integrated design aspects.

The FE analysis will establish the thermal strain induced by cooling the assembly from room temperature to -25°C, the gravitational sag without and with sectors, and the distortion in the ring from potential service loads. For lack of better definition at this point, the service load will be assumed to be a 2 N normal load midway between the ring support points.

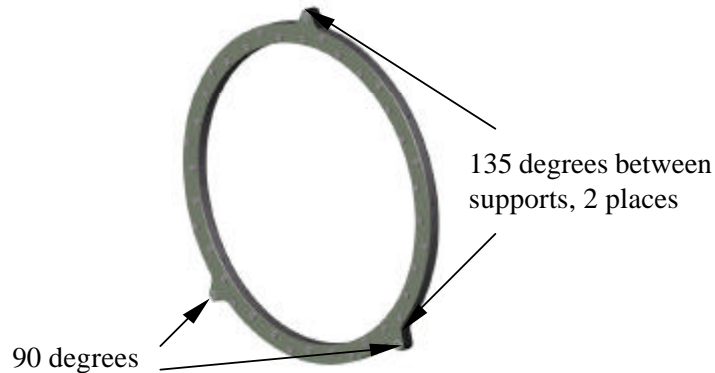


Figure 2: 3D illustration of the composite ring, showing the location of the 3 support points.

2. Discussion of Analytical Results

The property values and material thickness used for the ring materials is given in Table 1. The material facing thickness, Young's Modulus, Poisson's ratio, density, and coefficient of thermal expansion is given by the symbols, t , E , ν , ρ , and α .

Item	Material	t-mm	E-kg/mm ²	ν (Poisson's ratio)	ρ -kg/mm ³ X10 ⁶	α -ppm/K
Facing	P30 C-C	0.41	15029.4	0.301	1.674	-1.2
C-Channels	YSH50/CE	0.5	10232.8	0.341	1.738	-.23
Inserts	PEEK	¹	356.9	0.4	1.26	46.8
Inserts	C-C	¹	2883.4	0.3	1.9	10.9

Table 1: Material properties and component thickness used in composite ring study

Table 2 lists the weights for the individual components represented in the finite element model. Beam elements are used to model the PEEK inserts that span from the front to back face. The material weight for the flange on the PEEK insert and the bonded washer that connects the insert to the back face is not included in the model, nor is any

¹ Inserts for sector mounting are tubes with a wall thickness of 1.563 mm. Inserts for ring mounting are circular in cross section with a wall thickness of 1.543 mm.

stiffness benefit from these connections included. This is also true for the three PEEK inserts used for the ring mounting.

Item	Weight-g	Comments
Facing	43	Need to reduce weight by volume of insert hole pattern
C-Channels	67.9	Need to reduce weight by volume of hole pattern in skirt
Mount	22.2	C-C trapezoidal piece
Inserts	15.8	PEEK material, does not include bonded washer, or insert flange
Mount inserts	1.74	PEEK material, without bonded washer and flange, nor Al threaded inserts
Total weight	150.64	(weight of ring w/o adhesive is 159 g)

Table 2: Component weight breakdown reflected in finite element model

2.1 FEA Analysis of Support Ring

2.1.1 Support Ring Static Analysis

Thermal strains induced by cooling the ring from room temperature to -25°C are shown in Figures 3 and 4, radial and out-of-plane respectively. The ring is free to expand² or contract, depending on the negative or positive value of the material CTE. The PEEK inserts will contract in length, which produces a dimpling in the C-C face, a depression in Z of $17\ \mu\text{m}$ (Fig. 4). This depression causes a slight outward bowing of the C-Channel outer rim by $11.7\ \mu\text{m}$ (Fig. 3). Since the face depressions are nearly uniform, the out-of-plane motion of the sector should not be a significant problem. Later versions of the finite element model will explore this point. In addition, tests will be performed using holographic imaging that can precisely measure any out-of-plane movement.

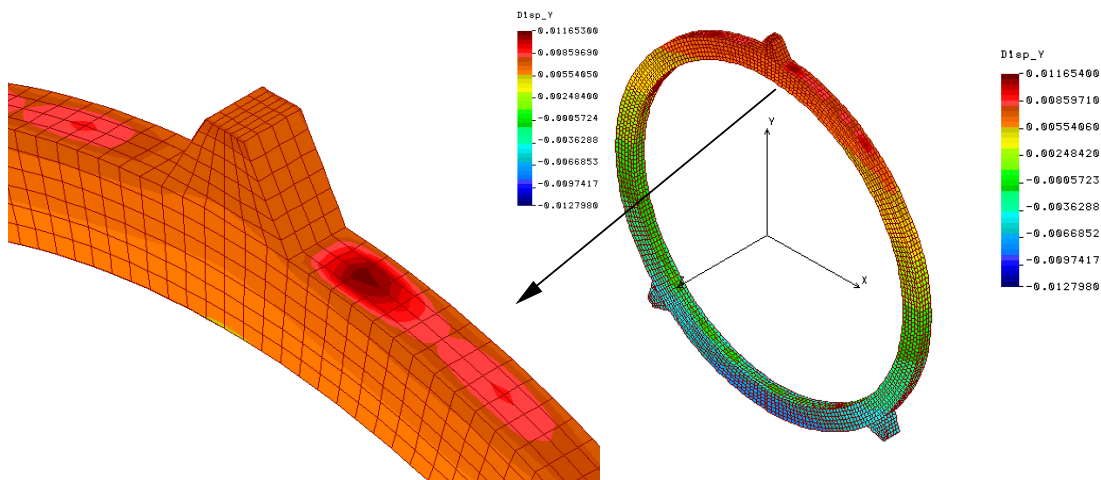


Figure 3: Left inset depicts the localized thermal strain in the C-Channel (radial direction) for temperature differential of 25 to -25°C . Peak strain is localized at points opposite to the PEEK inserts of 11.7 mm. Total radial change in shape for ring is depicted in right inset.

² No boundary conditions imposed on the ring three support points.

The negative CTE of the carbon-carbon facings cause the unrestrained ring to expand by 34 μm (Fig. 4).

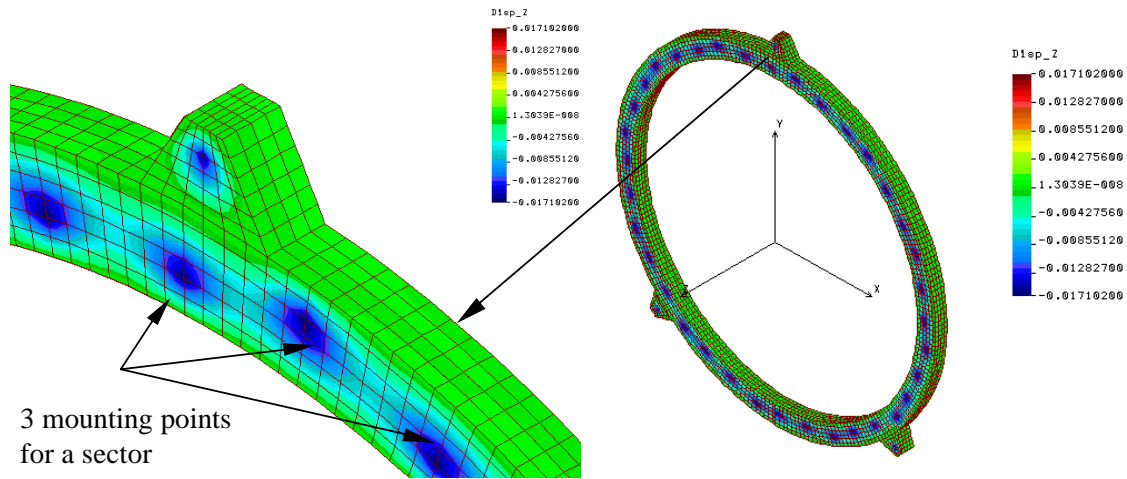


Figure 4: Left inset depicts the localized thermal strain in the ring facing for a temperature differential of 25 to -25 $^{\circ}\text{C}$. Peak strain from PEEK inserts is 17 μm . The thermal strain for the complete ring is depicted in right inset.

There are two mounting options being considered for the ring. The first option under consideration utilizes three adjustment screws mounted in three radial V-grooves³. The adjustment screw has a spherical ball at one end that fits into one of the radial V-grooves. This option is depicted in Fig. 5. This concept is being evaluated by machining radial V-grooves into an Invar plate. The Invar plate is a low expansion nickel alloy that will serve to simulate the low expansion composite frame that holds the V-groove mount.

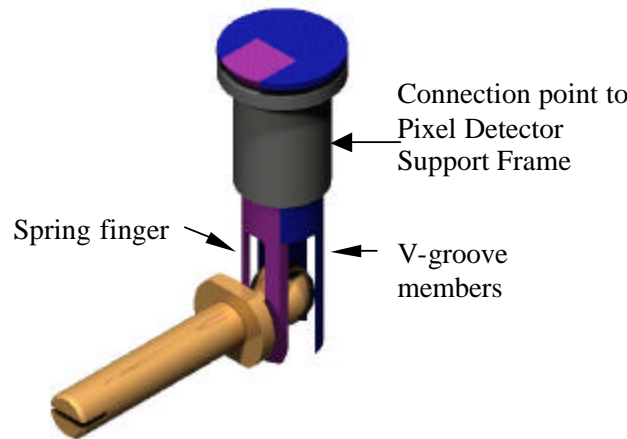


Figure 5: Illustration of a proposed mount for the disk composite ring. Ball on the end of an adjustment screw is spring loaded into a radial V-groove by a spring member.

The objective of the three radial grooves is to accommodate the difference in thermal expansion between the composite ring, the ring mount and Pixel Detector Support Frame. The plane of the V-grooves is located 5 mm behind the back face of the composite ring (support Case A).

³ V-grooves point toward the center of the ring

If the V-groove receiver were truly kinematic, a sliding motion would occur between the contacting elements, hemispherical ball and V-groove. However, stiction between the spherical ball and V-groove wall will result in some thermal strain being produced. In the FE model, we assume a pure kinematic condition; the three-point support restrains motion in X and Y by virtue of the lower radial V-grooves, and in azimuth, and Z. The vertical gravity load of the ring is carried by the two lower radial V-grooves. The vertical support point does not resist gravity because of the radial orientation of the V-grooves.

In the second mount option, no attempt is made to relieve thermal strains due to the thermal expansion mismatch between the ring and frame. The ring would be mounted on three radial mounts in the plane of the ring (support Case B). The compliance in the ring is used to accommodate the thermal strain. A variation in this concept employs an axial spring at the upper mount to reduce thermal strain.

The effects of both mounting conditions are analyzed. The objective is to assess ring stiffness, and robustness to withstand the estimated mechanical and thermal loads in the ATLAS Pixel Detector application, with these mounting options.

Fig. 6 graphically displays the out-of-plane ring distortion caused by the 1G gravitational load. The maximum out-of-plane distortion is 1.2 μm ; the peak occurs between the lower and vertical supports. As cited earlier the upper ring support does not resist the gravitational force, hence the vertical motion downward is a peak at this point. This effect is displayed in Fig. 7. The maximum vertical displacement for the ring alone is 1.4 μm .

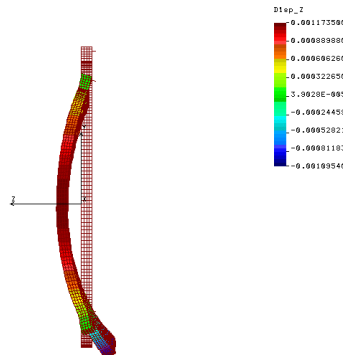


Figure 6: Effect of gravity sag in out of plane Z-direction for 1G load, strain in Y-direction. Peak displacement between supports is 1.2 mm. V-groove radial supports are located 5 mm from back face.

A 2-N load is used as a practical gage to assess the effect of anticipated service loads. A design limitation on this deflection has not been set yet, however, it is desired that the magnitude be consistent with the limits imposed for the pixel disk stability. A static load of 2-N concentrated at a node midway between the lower and vertical support, produces a peak Z displacement of 49.2 μm . This is shown in the left inset of Fig. 8 for Case A. Displacement shapes for the both Case A and Case B support conditions are shown in Fig. 8. The peak displacement for support Case B is 50.4 μm .

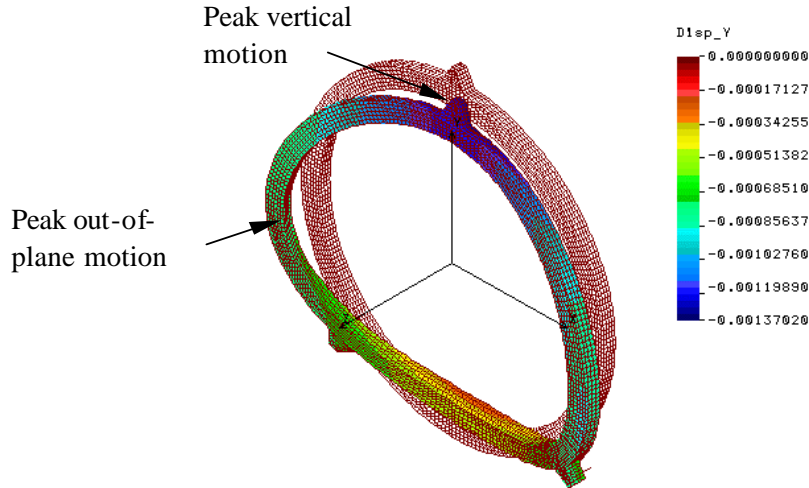


Figure 7: Gravity sag in vertical Y-direction for 1G load, strain Y direction. Peak gravity sag of 1.4 mm. V-groove radial supports 5 mm from back face.

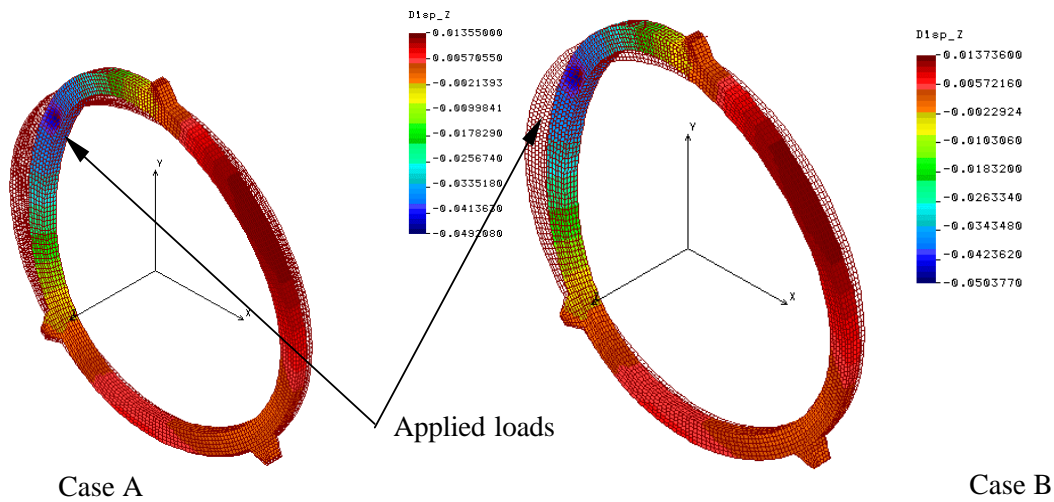


Figure 8: Resulting strain normal to ring face for a 2-N force mid-span between the upper and lower mounts for support Case A and Case B. The point of load application is the upper left quadrant for both support cases.

In radial mount concept (Case B), the weight of the disk is supported on two V-grooves in the lower quadrants of the disk. The axes of these V-grooves are tangential to the disk circumference. To eliminate motion, the upper mount (conical seat) will be fixed, or lightly spring loaded. The thought behind the latter approach is to minimize thermal strains induced by differential expansion between the disk and frame. To assess the sensitivity, i.e., radial stiffness, a concentrated 4.448 N (1 lbf) preload was applied to the upper support point. The ring distortion resulting from the concentrated load is shown Fig. 9. The peak displacement in the radial direction is 47.9 μm . Changing the inserts

that connect the two ring facings from the lower modulus PEEK material to a higher modulus carbon-carbon material ^[1] had no significant effect on the resultant distortion, Fig. 10.

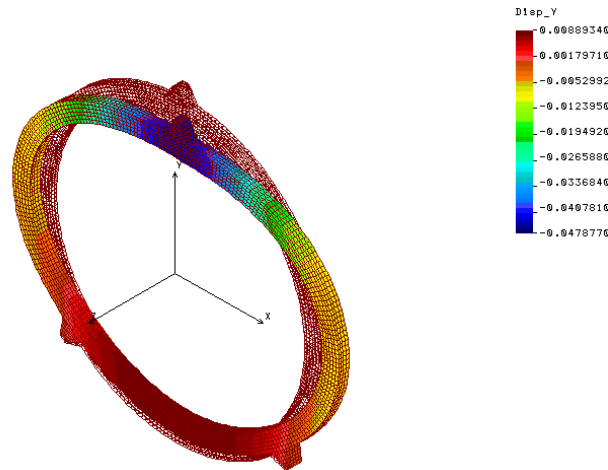


Figure 9: Radial strain induced by applying vertical load of 4.448 N at vertical mount of support Case B. Radial boundary conditions imposed at lower two supports restrain the ring against vertical motion. PEEK inserts are also being considered for mounting bushings in the sector composite sandwich.

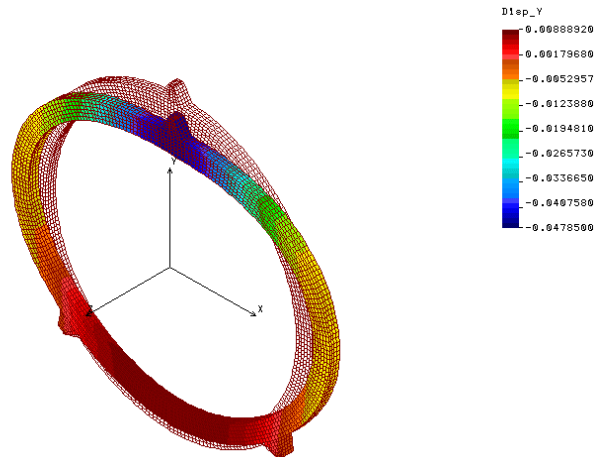


Figure 10: Vertical loading of 4.448 N at top radial support, with radial reactions at lower two supports. Property value for inserts changed from PEEK to carbon-carbon, without observable change in ring radial stiffness.

2.1.2 Support Ring (Only) Mode Shapes and Frequencies

The mode shape and frequency for the first four vibration modes were determined for the radial in-plane support condition. These results are shown in Figures 11 and 12. It is of interest to recall that the fundamental mode for the first support ring ^[1] was predicted to be 206.9 Hz, quite close to the 1st mode for this ring, in spite of the fact that the new ring is expected to be stiffer. The first ring had a facing thickness of 0.7 mm and a ring depth of 10 mm, whereas the present ring under construction has a facing thickness of 0.41 mm and a depth of 15 mm. The thinner facing material was chosen to be compatible with the thickness under consideration by LBNL for sector facings. This decision allows the residual ring material to be used for sector facings in the future. To

make up for the thinner facing in the present ring design and to gain additional stiffness, the radial skirt and the depth of the C-Channel was increased over the earlier design [1].

The boundary conditions used to simulate the radial, in plane ring mounts provide fixity at one node for each support. At all three nodal points the Z-direction, normal to the ring, is fixed. The lower two nodal points are fixed in the radial direction to provide vertical support, however, tangential to the ring the nodes are free to move simulating a V-groove. In contrast, the upper nodal point is free to move in the radial direction, but fixed in directions tangential and normal to the ring. The mode shapes provide evidence that small local rotations of the ring occur at the support points. It is quite probable that the specified boundary conditions have the effect of making the ring appear compliant.

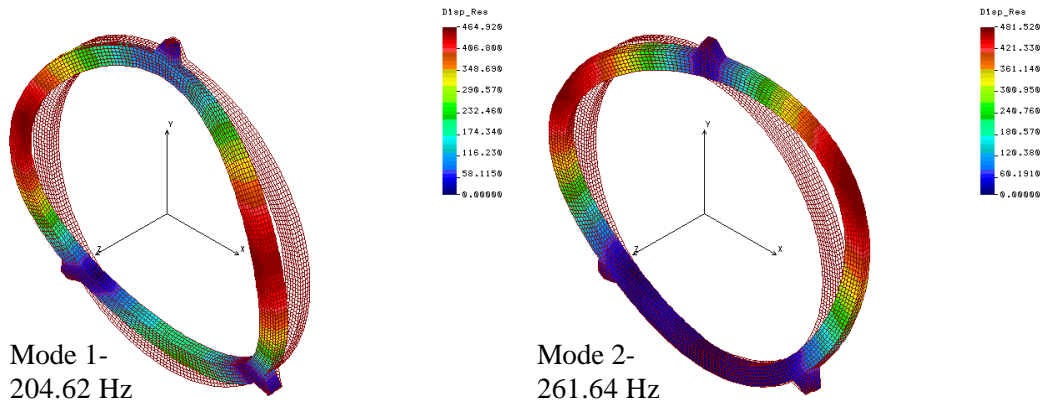


Figure 11: Dynamic solution for modes 1 and 2 of the support ring only. Support configuration is for Case B, i.e., three in-plane radial supports.

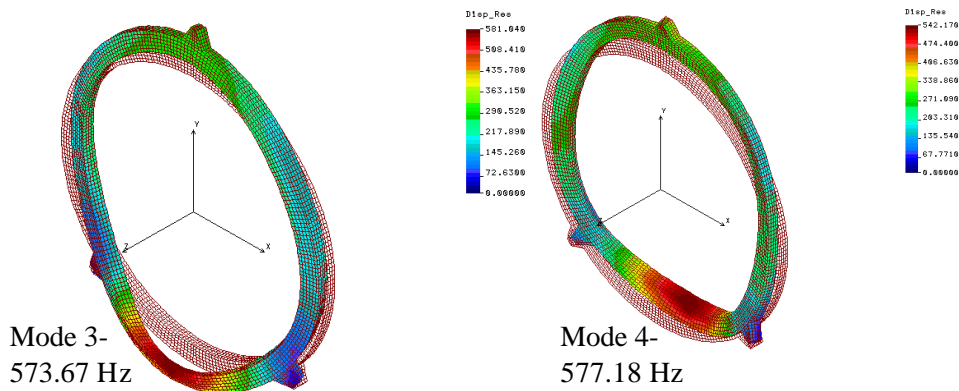


Figure 12: Dynamic solution for modes 3 and 4 for the support ring only, Case B.

2.2 FEA of Disk Assembly

2.2.1 Disk Assembly Mode Shapes and Frequencies

A finite element model was prepared for an individual sector to confirm the properties to be used in the simulation of the entire disk assembly. The physical parameters for the sector were quasi-isotropic carbon-carbon facings from P30 uni-tape, 0.41 mm thick, separated by 5 mm. The two facings are sandwiched with a carbon foam core with a 3% solid fraction. Total mass of the sector is 21.5g. The material properties

for this sector are listed in Table 3. The simulation is intended to fit the concept under consideration by LBNL⁴.

Item	Material	t- (mm)	E- (kgf/mm ²)	m (Poisson's ratio)	r- (kgf/mm ³) X10 ⁶	a- (ppm/K)
Facing	P30 C-C	0.41	15029.4	0.301	1.674	-1.2
Foam	ERG	5	7.074	0.30	0.064	2

Table 3: Sector model Material Properties

The first two modes for an individual sector are shown in Fig. 13. The sector is fixed at three points, corresponding to the mounting pin locations on the ring. The front and back faces of the sector are connected with beam elements simulating the mounting pins.

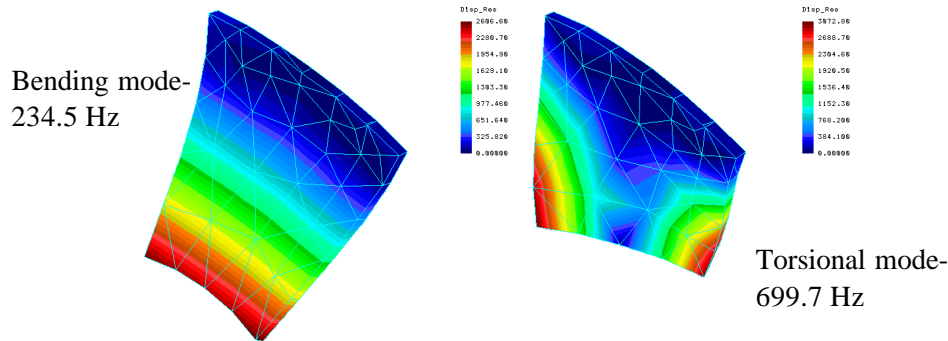


Figure 13: First two vibration modes for sector mounted at three points along the upper perimeter. Sector is a sandwich structure with carbon-carbon facings and a carbon foam core.

Vibration tests with an early version of the LBNL sector indicated the fundamental bending mode was in the range of 200 Hz. The sector simulation fits these early test results adequately.

The next step in the analysis is to structurally couple the sector FEM to the ring FE model, and then to assess the combined stiffness of the assembly. For the first simulation, we choose to prevent vertical motion at the upper ring mount (ball-in-cone). This solution will be followed by a solution wherein the *fixed* restraint is removed, and it is replaced with a spring that provides a preloaded mount condition.

The first four modes for a complete disk assembly are shown in Figures 14 and 15. As stated, the solution is for the radial mount condition, Case B, with a fixed radial restraint at the vertical mount location. Predominately the motion is out-of-plane, slight bending twisting of the ring and cantilever vibration of the sectors. This condition is quite evident between the upper and lower mounts (135° unsupported arc).

⁴ Tests of both the LBNL and HYTEC sectors indicate that the HYTEC sector is stiffer. It was judged appropriate to use a structural description that typifies the LBNL sector in validating the assembly stiffness; the presumption being that with the HYTEC sector, if anything, a gain in performance could be expected.

The proposed radial mount concept with a spring-loaded feature secures the disk, while providing a means for minimizing thermally induced strains. The justification for adding the compliance has not been established by a thermal analysis, and this aspect needs to be explored before a final appraisal is made. Our objective at this point is to evaluate the complication that may arise relative to the vibration modes of the disk assembly. Evaluating the ring dynamics with and without the spring boundary condition is posed as a means of addressing this concern.

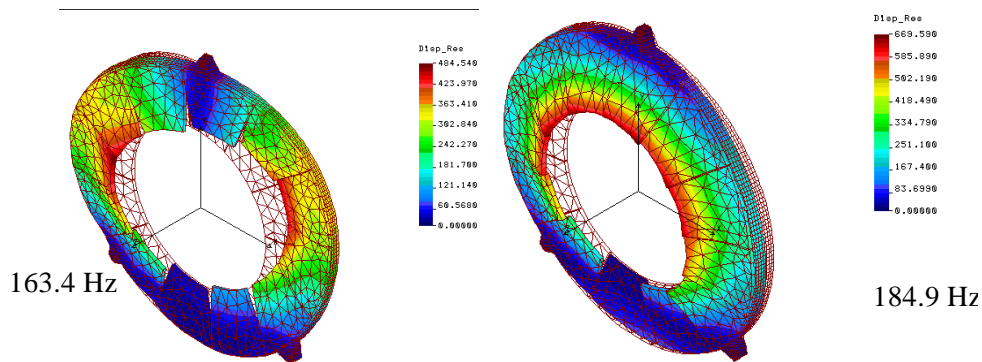


Figure 14: First two vibration modes for a complete disk assembly with 12 sectors. A *fixed* vertical restraint added at upper mounting point prevents vertical motion at the conical support. Bending and torsion of the ring is evident in the first mode. The second mode largely corresponds to the sector cantilever mode. The sector cantilever mode occurs at a lower frequency than depicted in Fig. 13 due to mounting the sector on a foundation with compliance (ring).

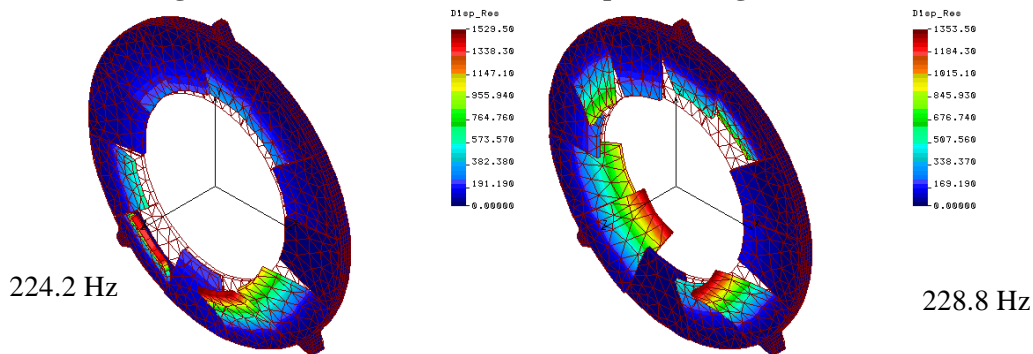


Figure 15: Vibration modes 3 and 4 for the 12-sector disk assembly for restraint Case B. Sector cantilever vibration modes are evident in modes 3 and 4.

To evaluate the effect of a spring at the top mount it becomes necessary to modify the radial restraint imposed at all three of the mounts. In the previous solutions, movement in the lower supports normal to the ring surface was fixed. If we were to leave this condition unchanged, we would negate the effect of a radial spring in the upper mount. Hence, boundary conditions in the form of local nodal restraints at the three mount locations are removed and replaced with 3D beam elements. The objective in using the 3D beam elements is to simulate the mounts in both axial and bending⁵. The beam axial stiffness direction is radial to the ring. Bending stiffness is normal to the

⁵ We are avoiding the use of gap elements, which simulate “lift off” of the ball in the V-groove. Vibratory motions of this amplitude are unacceptable.

beam axis in all directions; hence, this stiffness term provides restraint normal to the ring (Z), as well as tangential to the ring. Providing a bending stiffness term tangential to the ring, at first glance, would seem contradictory to the effect desired from the V-groove and spherical ball, Fig. 16. However, until *stiction* and/or the 1g disk inertia load are overcome at the spherical ball/V-groove contact point, no relative motion occurs. Under this condition, the dynamics of the ring/mount combination are set by the ring stiffness, and the mount bending and axial stiffness terms. To complete this argument, we must show ultimately that the vibratory motion is extremely low amplitude⁶ and that ring inertia is not overcome, and no relative motion occurs at this interface.

For the lower two mounts, the axial stiffness of the beam corresponds to an effective radial (axial) spring constant of 225 kgf/mm, Table 4. This preliminary value is used to simulate the axial stiffness of the lower mounts (radial direction) in the FEA of the ring dynamics. However, the precise value must be evaluated once the mount design is complete and the analysis updated accordingly. At the upper cone-ball mount, the axial stiffness of the beam element corresponds to a rather arbitrary radial spring constant of 2.25 kgf/mm (4.95 lb/in).

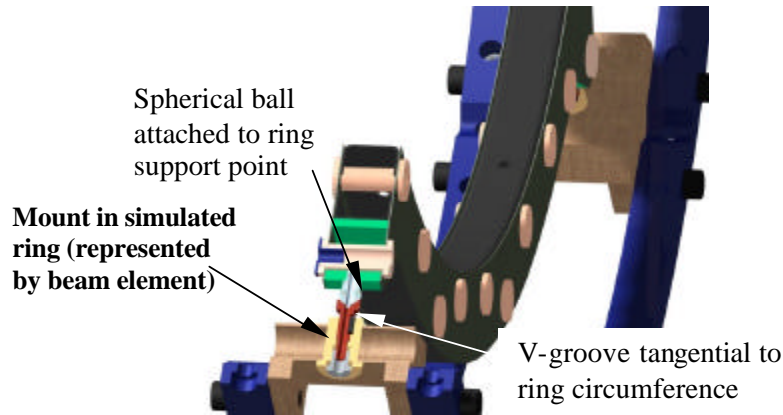


Figure 16: Lower ring mount cut-away, illustrated as part of the test set-up for the 12-sector disk assembly.

Mount	Axial stiffness (kgf/mm)	Bending stiffness (kgf/mm)	Young's Modulus (kgf/mm ²)	Axial area (mm ²)	Unsupported length (mm)	Moment of inertia (mm ⁴)	Effective Beam diameter (mm)
Lower	225	11.5	210.9	5.33	5	2.26	2.61
Upper	2.25	11.5	210.9	.0533	5	2.26	2.61

Table 4: Pseudo Mount Parameters

Table 4 lists the parameters that define the 3D beam properties. The dimensions listed for the pseudo mount are smaller than presently under consideration, hence the axial and bending stiffness values are expected to be higher than that used in the FEA of

⁶ If we assume that the vibratory motion of the ring is less than the ring distortion from the ring preload, contact will be maintained at the mount

the ring dynamics. The chosen Young's Modulus is representative of a plastic material, which is in keeping with our initial assumption that the mount will be fabricated from PEEK, or some similar plastic material. The axial area for the upper beam element, which simulates the spring, is reduced 100 fold over the lower mounts, however, the bending or tangential stiffness at the top remains the same as the lower mounts.

The first and second modes determined for the disk assembly with the 3D beam elements are depicted in Fig. 17. The resultant mode shape (Disp. Res.) reveals little motion at the three mounts. Most of the distortion occurs at mid span between the upper and lower mounts. Bending and twisting of the ring, combined with the cantilever bending of the sectors is evident. In the previous solution, the fundamental frequency without 3D beam elements was 163.4 Hz; it has now decreased slightly to 151.9 Hz. The mode shapes remain largely the same.

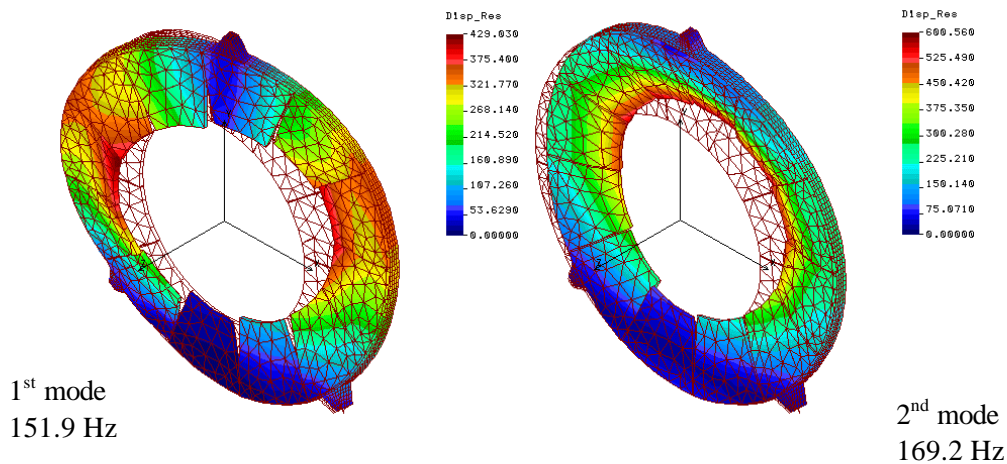


Figure 17: First two modes for a 12-sector disk assembly with a spring-loaded mount at the top. Presence of the spring results in a slight reduction in the first and second mode natural frequency. Both modes involve bending and twisting of the ring, quite unlike the FEA solution without beam elements simulating the mounts where the mode was characterized by vibration of the sectors.

These mode shapes are largely out-of-plane distortion as before. Distortions for out-of-plane and in plane are shown for the first mode in Fig. 18. The magnitude of vibratory motion out-of-plane is roughly a factor of 10 greater than for the vertical direction (Y).

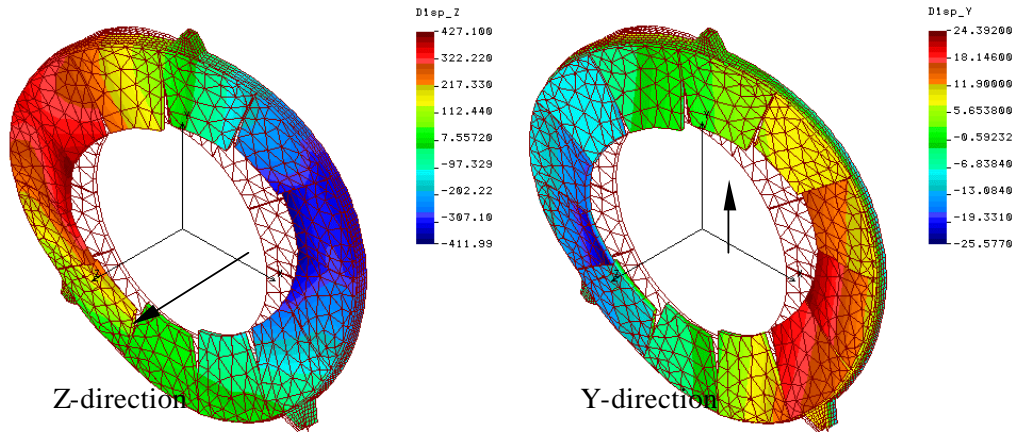


Figure 18: Vibratory distortion in the Z (normal to ring) and Y (in plane of ring) directions for the first mode (151.9 Hz).

It is possible to idealize the disk assembly supported by three radial mounts as a spring-mass system composed of three springs in series with a concentrated mass (disk assembly). One spring value represents the upper preload spring, the second representing the compliance of the disk assembly⁷, and the final spring representing the two lower mounts, which act as a pair of springs in parallel. This analytic model indicates that the frequency where a vertical rigid body motion of the disk occurs would not occur below 328 Hz.

The 16th mode is a rigid body motion of the disk assembly, a lateral and vertical motion of the disk in conjunction bending of the mounts (Fig. 19). The frequency of occurrence is 297.2 Hz, 9.4% lower than the estimate derived with a rather simple model. Resonance of individual sectors, typified by little or no motion of the composite ring, is responsible for the large number modes between the first four out-of-plane modes.

2.2.2 Disk Assembly Static FEA

Pre-loading the composite ring at the upper mount with a force of 0.454kgf (1 lbf) produces a deflection in the spring of 0.202 mm (2.25 kgf/mm rate). The spring force is directly transmitted to the ring ball/cone interface, which produces a lateral out-of-round motion (X-direction) in the ring of nominally 4 μm , left inset of Fig. 20. A 15.2 μm total vertical downward displacement of the ring at this point also occurs. Since a displacement of similar magnitude occurs at the ball/V-groove interface in the lower mounts, an effective shift in the disk central position of nominally 10 μm occurs. The difference in the Y displacement between the upper and lower is .0152-.0101=0.0051 mm. This 5 μm difference is the extent of out-of-roundness in the ring in the vertical direction, a narrowing of the ring. This deflection is quite similar in magnitude to the X-direction displacements, which corresponds to an expansion of the ring.

⁷ Spring value representing disk compliance is obtained from a static solution of the disk for boundary restraint Case B. Unit load is applied vertically downward and maximum deflection noted.

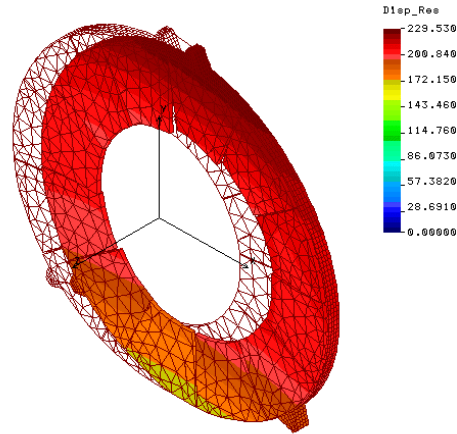


Figure 19: Rigid body vibratory motion of the disk assembly on the pseudo radial mounts, using 3D beam elements (Table 4).

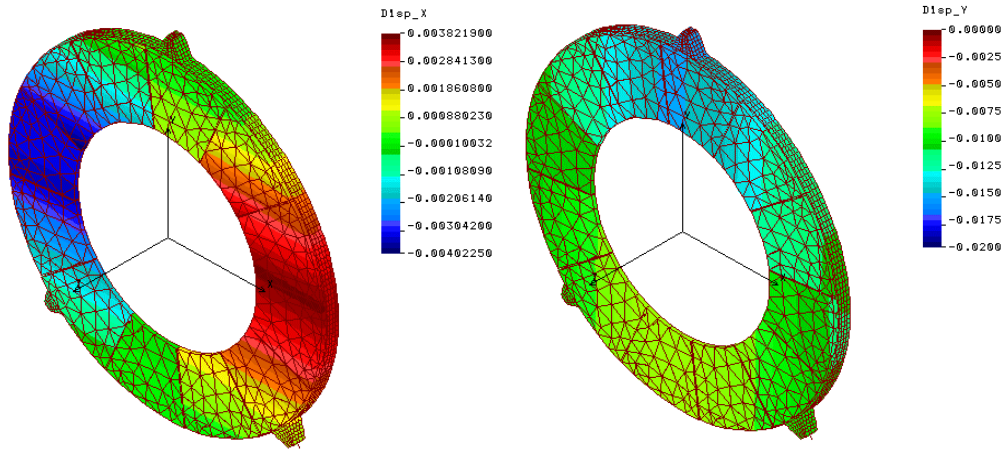


Figure 20: Static solution for 4.448N (0.454kgf=1 lbf) axial spring force applied at upper mount. Left inset depicts the lateral X-displacement and the right inset the vertical Y-displacement of the ring and sectors.

A force of 2-N was applied normal to the model of the disk assembly at mid span between the upper and lower mounts, the same condition previously solved with the bare ring. Both solutions are for mounting condition Case B. The out-of-plane ring distortion decreased slightly, Fig. 21, the peak deflection being 0.048 versus 0.050 mm. For this particular loading condition, we conclude the sectors provide very little reinforcement to the ring. The simulation used a fixed Z restraint at the node where the 3D beam elements join the ring. This boundary condition prevented the bending stiffness of the individual mounts contributing to out-of-plane displacements, so that a direct comparison with the previous solution could be made. In Fig. 21 (right inset), we also show the result with this Z-restraint removed, introducing the compliance of the simulated mount. The Z-deflections at the three mount connections are: -0.003 upper, -0.0038 lower left, and +0.0099 right side; all displacements are in mm. The mounts denoted upper, and lower left are closer to the applied load than mount denoted *right side*.

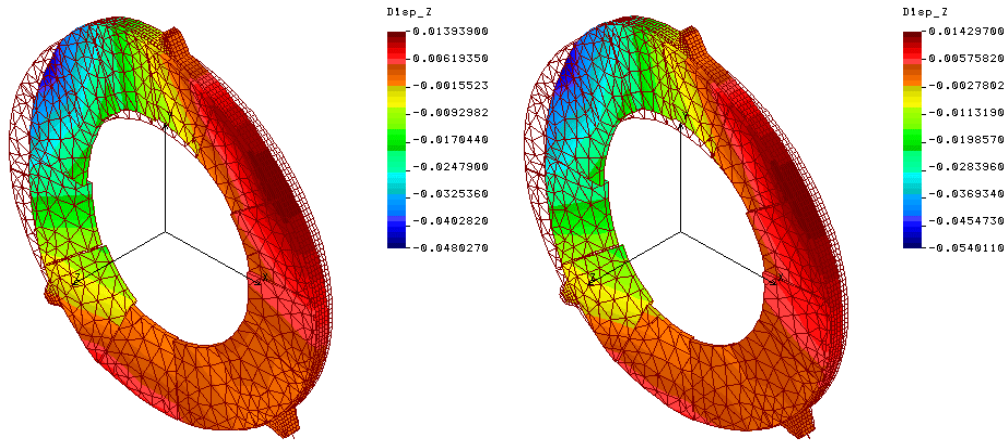


Figure 21: Static solution for force of 2-N applied mid span between upper and lower left mounts for a 12-sector pixel disk assembly. Figure at left has the bending compliance of the mounts removed. Figure at the right includes the bending stiffness for the mounts used in previous solutions.

2.2.3 FEA of Disk Assembly Thermal Strains

The FE model used to establish the static and dynamic stiffness of the disk assembly was subjected to a temperature change of 45°C. The objective of this solution is to develop some measure of the differential contraction and expansion effects from the various materials comprising the ring. The distortion of the assembly is shown in Fig. 22. The distortion out to the middle of the sectors is for the most part 10 μm or less. From the middle of the sectors to innermost radius, the distortion increases up to a maximum of 97.5 microns. Since the sector FE model does not include the stiffness derived from sandwiching of the C-C cooling tube, it is reasonable to expect that the actual distortion will be much less⁸. Thermal strain measurements for the HYTEC Sector mounted on a simulated ring are much less than suggested by this simplified FE model. The most that can be deduced from this solution is that the different component materials, i.e., C-C facings, YSH50 C-channels, and PEEK inserts, making up the ring are causing large local distortion in the vicinity of the ring perimeter.

⁸ LBNL Sector design structurally decouples the aluminum tube from the sector facings. It is possible that the distortion of this sector on the mounting ring will behave as shown in Fig. 22.

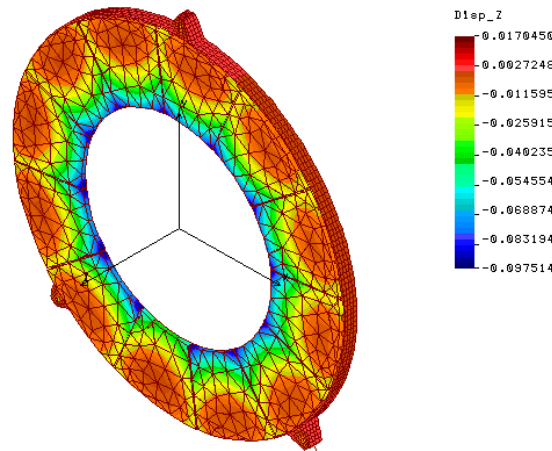


Figure 22: Thermal strains for Disk Assembly for temperature change from 25°C to -20°C. Support conditions reflect 3 point in-plane radial mounting of the ring, Case B.

Future FEA work on the disk will be directed toward improving the model of the sector properties. Although the simulation of the Triple U-tube is a rather difficult object to model, an incentive exists to improve our understanding of the structural behavior of the sector.

3. Summary and Recommendations for Future Work

A preliminary finite analysis of the composite material ring for supporting the ATLAS Pixel Detector sectors is nearing completion. The ring FEA included an evaluation of two proposed ring mounting concepts, both three point mounting. For each mount concept, the imposed boundary conditions and mount simulation technique restrained the ring in translational degrees of freedom. The proposed mount connections to the ring supports do not transfer moments, and the model simulated “ball in a V-groove, and/or ball in a cone type interfaces”.

The fundamental vibration mode of a 12-sector disk assembly, based on the ring construction details, is 151.9 Hz⁹. This solution is for a three-point mount, located in the plane of the ring. This frequency is well above the design goal of 100 Hz for the ATLAS Pixel Detector.

Imposing a load (2 N) normal to the ring at mid span between support points is used as a static measurement of ring stiffness. This load produced a deflection of nominally 50 μm ¹⁰ in a 12-sector disk assembly. A similar solution without sectors, ring only, yielded nominally the same magnitude. For this particular loading condition, the presence of the sectors does not enhance the stiffness of the ring.

The preliminary FEA of the ring included a determination of thermal strains induced by cool-down from room temperature to -25°C. The distortions in the ring were

⁹ Direct performance comparison between an earlier composite material ring, constructed for ESLI, is difficult. However, a 12-sector disk assembly with this ring had a natural frequency of 115.4 Hz. This implies the ring constructed for the HYTEC SBIR is over 70% stiffer. The objective behind the new ring construction details was to achieve at least a 150% increase.

¹⁰ FEM model of ESLI ring alone is 103 μm ; this implies a stiffness increase of roughly 100%.

small, nominally 12 μm . A similar solution is for the 12-sector disk assembly was made and the out-of-plane distortions in the ring area reduced to roughly 5 μm . Distortions in the sectors reached a peak of 97.5 μm . There is reason to believe that this effect is caused by not simulating the presence of the cooling tube in the sector sandwich.

The results from this analysis will be compared with structural testing of the ring and disk assembly. Part of the future study effort will be to reconcile our analysis with the test results.

4. References

[1] F. Biehl and W.O. Miller, ATLAS/ESLI Mounting Ring Plus Detector Sectors Thermoelastic Static and Modal Analysis, HYTEC-TN-ESLI-03, dated April 10, 1999.

Static and Modal Testing Of Composite Support Ring for a Pixel Detector Planar Array

W.O. Miller, G. Hayman, R. Baer, W.K. Miller
HYTEC, Inc.
June 1, 2000

Abstract

This report covers the preliminary experimental testing performed on the composite ring used to support carbon-carbon thermostructures for a pixel detector. Development of the thermostructure is supported by a Department of Energy Phase II SBIR. The mounting ring is hollow, consisting of carbon-carbon (C-C) face sheets separated by PEEK posts and edge closeouts constructed from a resin based composite material. The ring is supported at three points around its perimeter during static testing. A free-free support of the ring was used for the dynamic testing.

TABLE OF CONTENTS

1. INTRODUCTION..... 3

2. RING CONSTRUCTION DETAILS..... 4

3. COMPOSITE RING DYNAMIC AND STATIC TEST RESULTS 6

 3.1 PRELIMINARY DYNAMIC TESTING..... 6

 3.2 RESULTS OF PRELIMINARY COMPOSITE RING STATIC LOAD TESTS 9

4. REFERENCES..... 10

1. Introduction

The primary objective of the “*Ultra-Lightweight Carbon-Carbon Cooling Structure for Pixel and Silicon Strip Detectors*” Phase 2 SBIR is to develop an ultra-lightweight, highly stable structure for supporting and cooling a flat panel array of pixel modules. The structure, entitled *thermostructure* is being proposed by HYTEC for use in the ATLAS Detector, one of two detectors scheduled for the Large Hadron Collider experiment. As part of the SBIR, HYTEC is to design and test a composite ring for supporting the thermal structures (sectors) in a disk-like arrangement.

This technical note presents the preliminary experimental test results obtained using a precision holographic imaging system. The tests are for both static and dynamic conditions. The static test provides a measure of ring stiffness, while the dynamic test provides information on the ring vibration modes. A secondary objective of the testing is to provide a confirmation of the finite element modeling used in the design of the ring. The primary analysis of the ring is reported in [1].

The composite ring is a box-like structure composed of a front and back carbon-carbon facing bonded together with C-Channels located on the inner and outer ring periphery. A 3D model of the ring is shown in Fig. 1.

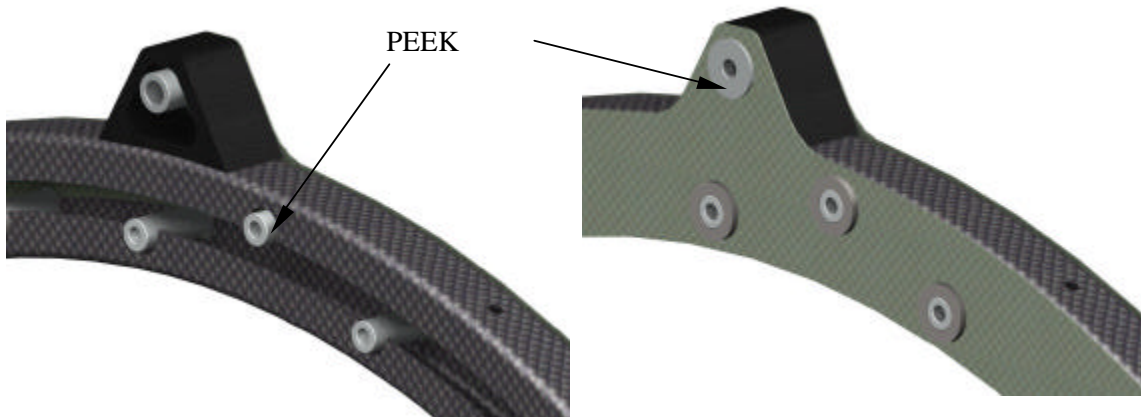


Figure 1: Left inset is an illustration of the inner and outer C-Channels for the composite ring, front facing removed. Right inset depicts the back facing installed and the bonding of the PEEK washers to the back face.

The ring and 12 sectors comprise a disk assembly. This assembly is supported at three points on its periphery. Fig. 2 is a view of the assembly with the 12-sectors removed. The support points in the lower two quadrants support the gravitational load imposed on the disk. The upper support point, in its final configuration, will provide rotational restraint about an axis normal to the ring (Z). All three points restrain the ring in a direction normal to the ring (Z).

The final structural design of the ring is influenced to a significant extent by the method used to mount the disk assembly in the pixel detector outer frame. Although, the design of the mounts (a local support issue) is not part of this SBIR effort, it is important that this element be considered in the design of the ring. As a first step, the support

boundary conditions chosen for the ring testing will emulate only the reaction at the ring and the mount interface. In the final analysis, the compliance in the mount and the support frame must be included in any structural representation of the pixel disk assembly. The complete model is needed to verify the integrated design aspects.

The tests planned will establish the thermal strain induced by cooling the assembly from room temperature to -25°C , and the distortion in the ring from potential service loads. For lack of better definition at this point, the service load will be assumed to be a 2 N normal load midway between the ring support points.

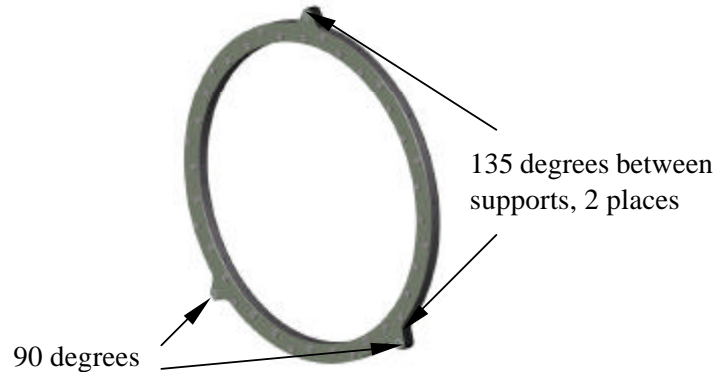


Figure 2: 3D illustration of the composite ring, showing the location of the 3 support points.

2. Ring Construction Details

A photograph of the completed ring is shown in Fig. 3. The ring is shown placed over the Invar test support fixture. Three fasteners attach the ring to the test plate; these fasteners incorporate hemispherical seats to engage V-grooves machined in the test plate. The objective of this mounting arrangement is to avoid transferring moments to the ring, as well as to accommodate differential contraction and expansion effects between the ring and test plate. Normally the hemispherical seats on the fastener are spring loaded to the plate. However, for the initial testing of the ring, the spring was removed, and the ring was mechanically pulled down into the V-groove with a threaded nut. Fig. 4 is a photograph of the hemispherical seat on the fastener that is threaded into the ring.

Table 1 lists the weights for the various elements that made up the ring. The total before bonding was 159g. After bonding, the ring weighed 180g.

Item	Description	Weight-(g)
1	Bottom face sheet (sector side, Qty 1)	23.42
2	Top face sheet (Qty 1)	23.73
3	PEEK inserts (Qty 36, plus 3 mounting inserts)	25.89
4	PEEK washers for inserts (Qty 36)	5.29
5	Inner and Outer C-Channels (Qty, 2 each)	61.29
6	C-C mounting blocks (Qty 3)	17.65
7	Weight of scab plates	2.10
	<i>Total dry weight</i>	159.37

Table 1: Ring Component Weight Breakdown

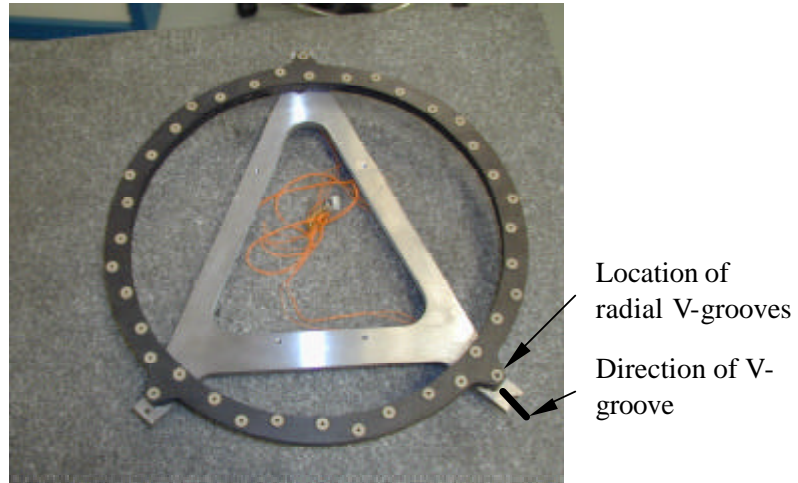


Figure 3: Photograph of the composite ring mounted on Invar test fixture. Mount attachment at three support points using hemispherical ball seats in radial V-grooves.

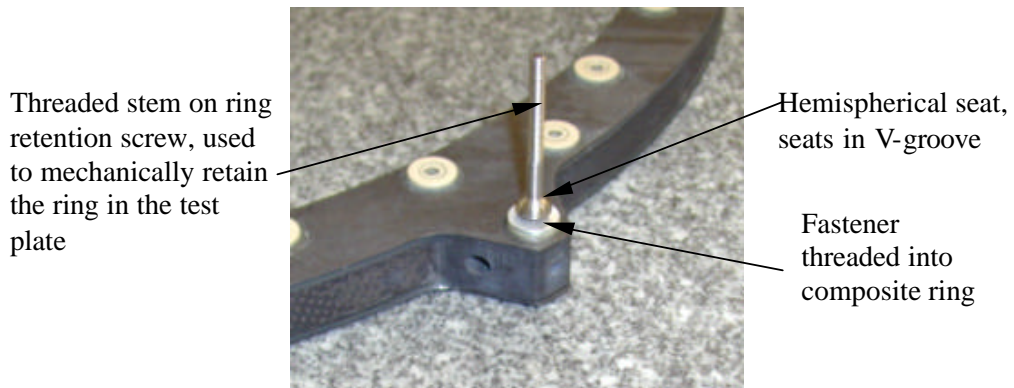


Figure 4: Photograph of hemispherical seat on threaded fastener protruding from the composite ring.

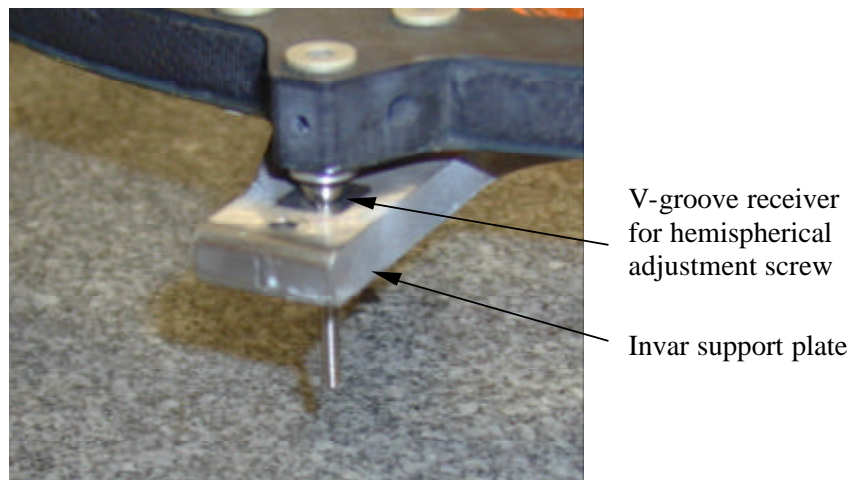


Figure 5: Photograph of the mounting interface between the composite ring and the Invar support plate.

3. Composite Ring Dynamic and Static Test Results

3.1 Preliminary Dynamic Testing

Experimental determination of the composite ring's mode shapes and resonant frequencies was performed with the HYTEC PRISM system, a laser-based holographic imaging system used extensively for static and dynamic structural evaluations. Processing of the fringe data from PRISM provides a graphic illustration of the vibratory mode shape. The structure is excited with a small PZT device, with the driver being swept through a wide frequency range until a resonant frequency is encountered. Throughout the frequency spectrum of excitation, PRISM provides information needed to evaluate the ring change in shape. The shape changes are evaluated by comparing to distinct holographic images. By storing images at discrete frequencies, it is possible to extract dynamic response on either side of the resonant frequency, as well as establishing the modal displacement at resonant. This information can be used to establish the structure's modal damping.

This procedure was applied in evaluating the ring dynamic response, when mounted on the Invar plate. However, during the initial ring testing considerable difficulty was experienced in separating the ring natural modes of vibration from that of the Invar plate and associated support structure. It was problematical that a quick solution could be found to suppressing these modes of vibration. A rather hurried decision was made to proceed with an attempt to determine the composite ring fundamental mode in a "free-free" state, i.e., no restraints. Actually, knowledge of the fundamental ring mode is quite helpful in validating the FE model of the composite ring.

To simulate a free-free boundary condition the ring was removed from the Invar mounting plate and rested on foam. To clear the Invar plate, it became necessary to rotate the ring counterclockwise a small amount, thus avoiding contact with the V-groove receivers. Figures 6 and 7 illustrate the fringe data for the first two modes established with PRISM.

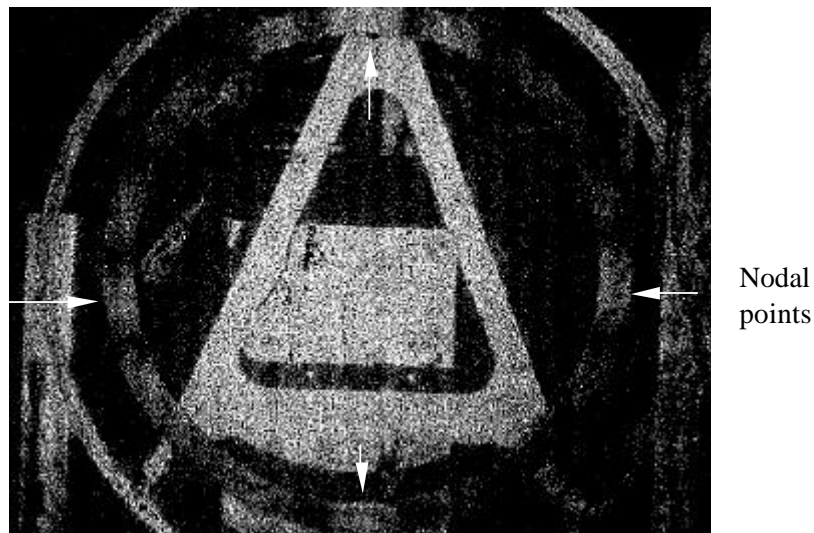


Figure 6: Holographic fringe pattern corresponding to the fundamental, "free-free", composite ring vibration mode is shown with the arrows pointing to the nodal points. Frequency was observed to be 330 Hz

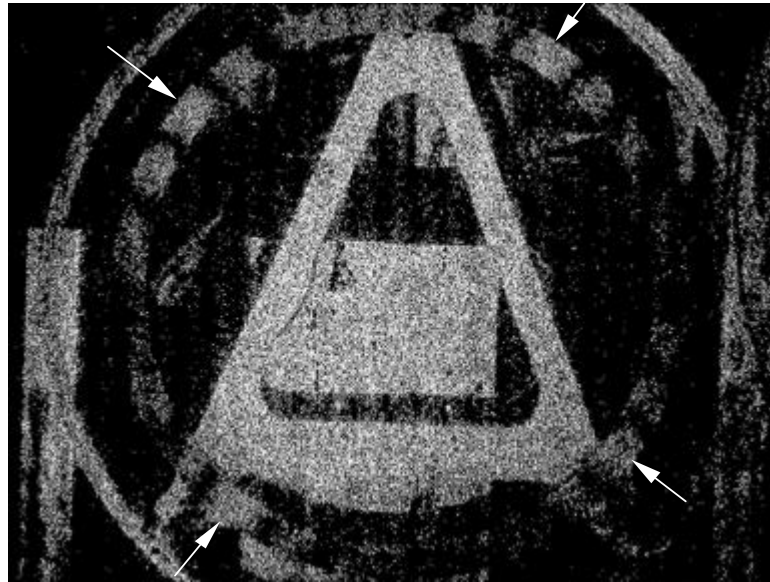


Figure 7: Holographic fringe pattern corresponding to the second, “free-free”, composite ring vibration mode is shown. The frequency associated with the fringe pattern is 352 Hz

Corresponding predictions were made using the HYTEC composite ring finite element model. This model was used to predict the ring structural behavior presented in [1]. The modal frequency analysis derived from the FE model is shown in Figures 8 and 9. The mass of the structure reflected in the FE model understates the actual recorded ring mass by a significant amount. The actual ring mass was 180g, whereas the model reflected a mass of 151.9g. A large contributor to the difference was found to be associated with the mass represented by adhesives.

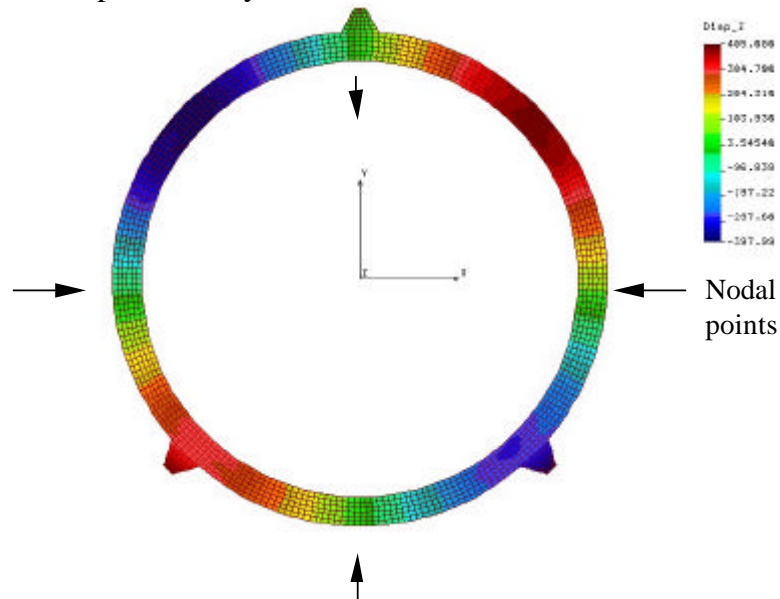


Figure 8: FEA prediction of “free-free” vibration mode for the unsupported composite ring is shown. First mode is 347.59 Hz. FE model is presented in [1].

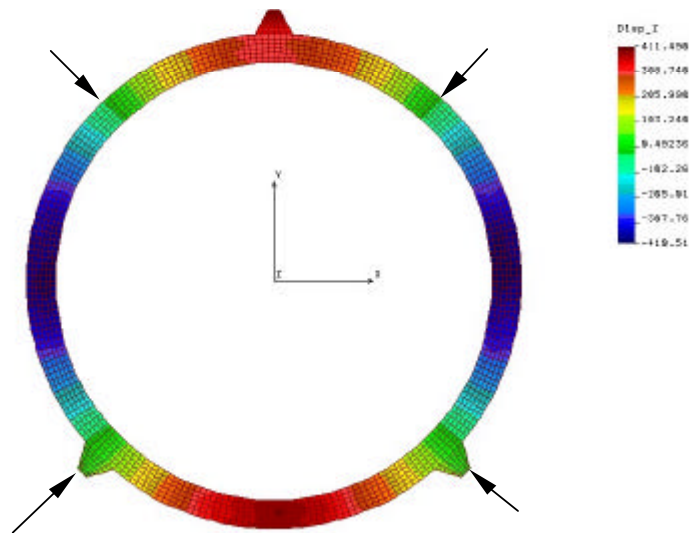


Figure 9: FEA prediction of second “free-free” vibration mode for unsupported composite ring with nodal points denoted. Second mode is 371.03 Hz. Ring mass represented in the FE model is 151.9g.

Table 1 compares the predicted resonant frequencies with those determined from the preliminary ring test. It is interesting to note that the predicted frequency is nominally 5.0% higher than the observed frequency for each mode. This situation is consistent with the model ring mass being lower than the actual ring mass.

Table 1 Comparison between observed and predicted resonant frequencies for the composite ring in a “free-free” boundary condition.

Modal Description	Recorded Resonant Frequency-Hz	Predicted Frequency-Hz	% Difference
Fundamental mode	330	347.59	5.33
Second mode	352	371.03	5.41

The mass representation in finite model was modified to allow for the mass associated with the adhesives used in constructing the ring assembly. The adjustment to the model was made simply by increasing the density of the ring C-C facings. This artifice is far from exact, but judged reasonable for a first cut. The change in the predicted resonant frequency is shown in Table 2.

The increase in ring mass changed the frequency proportional to roughly the mass ratio $\sqrt{\frac{M_o}{M_n}}$, where the subscripts *o* and *n* represent the old and new ring masses. The underlying assumption is that the approximation to such a change is governed by the fundamental relation for a single degree of system, i.e., the frequency is proportional to $\sqrt{\frac{K}{M}}$, where *K* and *M* correspond to the system stiffness and mass. Taking this a step further implies that the finite element model is under predicting the composite ring stiffness by 1.053², or roughly 10.9%. The next step is to watch for this effect in the analysis of the static testing of the ring.

Table 1 Comparison between observed and predicted resonant frequencies for the composite ring in a “free-free” boundary condition.

Modal Description	Recorded Resonant Frequency-Hz	Predicted Frequency-Hz	% Difference
Fundamental mode	330	317.03	3.93
Second mode	352	335.88	4.58

3.2 Results of Preliminary Composite Ring Static Load Tests

A static load test was conducted by applying a concentrated load on the ring at mid span between the two adjacent supports, and midway between the outer and inner ring radii. For this test, the composite ring was mounted on the Invar support plate using the three radial V-groove mounts; support Condition Case A of [1]. The contact area of the point load was 2.29mm; the point of contact was within 0.635mm of the theoretical midpoint.

The fringe pattern obtained with the HYTEC Prism system for the concentrated load test is shown in Fig. 10. For this case the applied load was 550mN. Load application proceeded incrementally, until a total 1.568N load was achieved. Fringe data was processed at roughly 500mN steps. A maximum deflection of 26.3µm was reached at the 1.568N load condition.

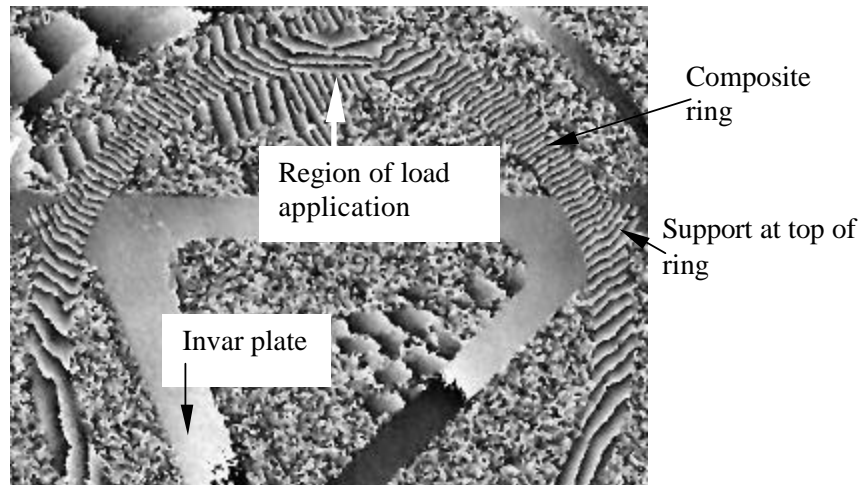


Figure 10: Display of fringe pattern for 0.55N load applied to middle of composite ring half way between ring supports. Ring is supported on Invar plate using the three radial V-groove mount concept. Maximum deflection at point of application is nominally 2.42mm.

Reference [1] contains an FEA solution (support Case A) corresponding to this loading condition. For a 2N concentrated load, the FEA prediction 49.2µm (peak displacement) can be linearly adjusted to 38.57µm at 1.568N¹. The test result is however quite a bit lower, 31.8% lower than the prediction to be exact. The dynamic tests

¹ Extrapolating the FEA prediction down to the test load case is reasonable since the solution is for a linear system.

suggested the model stiffness is underestimating the ring stiffness, however, only by 10.9%. Adjustments to FEA of 10.9% would be expected to diminish the predicted result at 1.568N to 34.37 μ m. Even after this adjustment, the preliminary experimental data would be still 23.5% lower. Other reasons for explaining this large difference need to be identified and explored. One natural area would be to re-examine the boundary conditions (BC) imposed to simulate the three-point, radial V-groove mount. In the present FEA simulation the BC imposed attempts to emulate kinematic mounting, i.e., some sliding at the contact points are allowed. At a low ring load this may not occur. This area will be investigated next, along with an attempt to explain the difference in stiffness between the FEA and the preliminary test result. Also, additional tests are recommended to confirm the measurements.

4. References

[1] W.O. Miller, Thermoelastic Static and Modal Analysis of Composite Support Ring for a Pixel Detector Planar Array, HTN-106020-0001, dated June 1, 2000



Analysis of ATLAS Disk Support Ring 432mm Global Support Structure

W. O. Miller
April 22, 2001

Abstract

The ATLAS-LHC pixel disk support ring has been re-designed for the recent size reduction in the Global Support frame. The support ring design also incorporates 4-radial support points, in lieu of three points used in the 500mm frame prototype ring. The prototype ring was constructed with PEEK bushing material, which is used to support and precisely locate the individual sectors, 12 in all. The new ring concept, in addition to being smaller in diameter, provides mounting for 8-sectors. A finite element model was prepared for the new ring concept to evaluate the ring stiffness and to quantify the benefit of changing the sector mounting bushing to a 3D carbon-carbon material. The prototype ring used PEEK bushings to facilitate manufacturing, however, the material high thermal expansion property is not well matched to the other ring composite material properties.

DESIGN ENGINEERING
ADVANCED COMPOSITE APPLICATIONS
ULTRA-STABLE PLATFORMS

110 EASTGATE DR.
LOS ALAMOS, NM 87544

PHONE 505 661-3000
FAX 505 662-5179

Table of Contents

<i>1. Introduction</i>	3
<i>2. Discussion</i>	3
<i>3. Conclusions</i>	8

1. Introduction

A finite element model was constructed directly from the Solid-Works (SW) 3D CAD file of the ring geometry under consideration for ATLAS. COSMOS/Works, a seamless interface of COSMOSM and SW, was used to mesh the problem and for running the thermal strain and static analysis solutions. The model uses solid tetrahedral-elements for the representation of all the components comprising the ring. It is acknowledged that the ring facings, and outer and inner C-Channels are thin walled structures, and that use of 4-noded tetrahedral-elements can affect the solution accuracy. However, this approach was used to achieve an expedient solution, avoiding the time consuming regeneration of the geometry using shell elements.

2. Discussion

The first solution step was to solve for the ring distortion from by applying 1N of force normal to the ring arc, which spans between two supports. Due to limitations in COSMOS/Works the load had to be applied to bushing contact points, not at the desired radial mid point. Thus, the force is slightly off center radially, since the chosen bushings are nearer to the inner radius of the ring. The boundary conditions used at the four supports points simulate a fixed radial and tangential condition. This fixity simulates the mounting of the spherical balls located on the ring in conical seats.

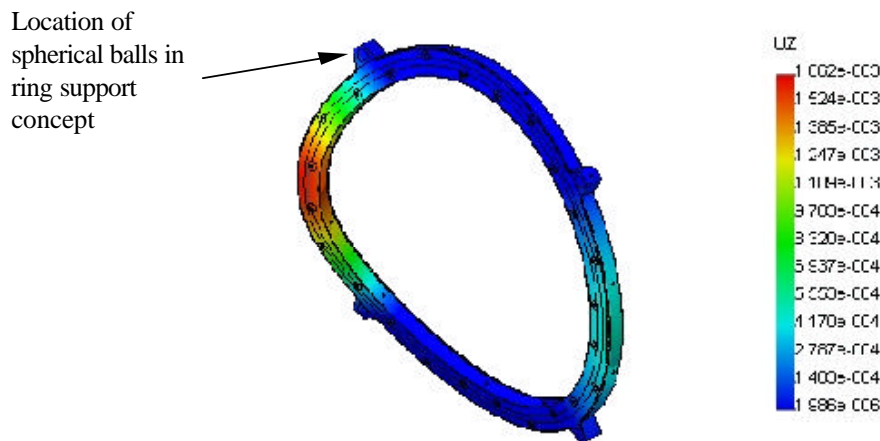


Figure 1: Displacement normal to ring cross-section due to 1N applied load. Load application uniformly applied over two bushings in center of ring arc. Displacement units are mm; maximum displacement is nominally 1.66mm.

Figure 1 depicts the solution for the applied load. The resulting peak distortion is nominally $1.66\mu\text{m}$. Scaling actual test data from the larger diameter ring to the smaller ring diameter, in addition making an allowance for the shorter span between support points, yields a displacement reasonably close to the predicted value. The ring compliance extracted from the above solution is $1.66\mu\text{m}/\text{N}$, whereas for the larger diameter ring the compliance was measured to be $16.8\mu\text{m}/\text{N}$, (versus prediction of $23.5\mu\text{m}/\text{N}$ using shell elements). As cited, scaling the measurements made with laser interferometry (HYTEC PRISM system) to the geometry reflected by the present ring design, will yield an estimated compliance of $2.67\mu\text{m}/\text{N}$ (versus FEA value of 1.66). It is possible that the mesh could be finer, possibly improving the correlation. However, at this stage of the ring design this correlation is considered adequate.

Figure 2 through Figure 5 show the thermal distortion in the ring for various directions, including the overall resultant motion. The distortion is due to cooling the ring from room temperature (25°C) to -15°C , with fixed constraints at the 4-mounting points. The out-of-plane (Z) distortion caused by the PEEK bushing inserts is quite evident in Fig. 2. This is the direction that the thermal strain is largely unaffected by the boundary conditions. The peak contraction toward the ring mid plane occurs at the mounting interface with the sector, a contraction of $19.3\mu\text{m}$. The contraction in the overall length of the bushing predicted by the FE model agrees very well with our expectations. The FEA further indicates that an individual bushing face does not remain flat, but rather distorts in a manner that might lead to tilting of the sector in the Z-direction (along detector axis).

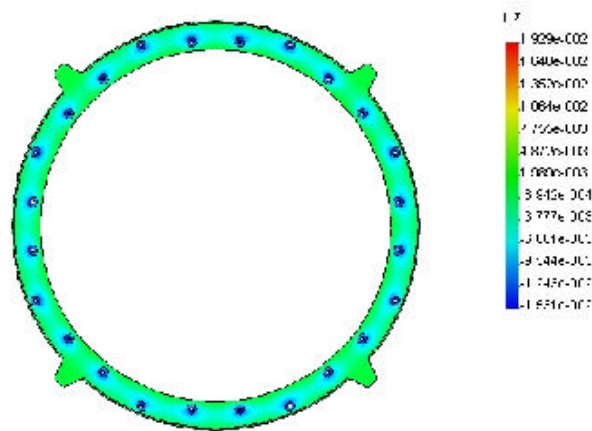


Figure 2: Bushing contraction in Z direction (PEEK Inserts) due to uniform temperature change from room to -15°C . Peak out-of-plane distortion at bushing/sector interface corresponds to $19.3\mu\text{m}$.

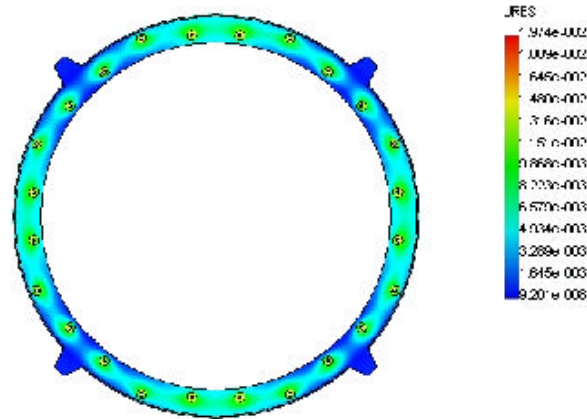


Figure 3: Ring (PEEK Inserts) resultant distortion from uniform temperature change from room temperature to -15°C. The peak distortion is concentrated in the contraction of the bushing faces.

Figure 4 and Figure 5 show the extent of the radial thermal distortion in the constrained ring. The peak distortion that occurs between supports is nominally $6\mu\text{m}$. It becomes apparent that this particular orientation for the three sector mounting points result in a corresponding in-plane rotation of the sectors (ϕ). This conclusion is drawn from the fact that no three mounting points move equally. A $6\mu\text{m}$ rotation across the three mounting points will cause roughly $6\mu\text{m}$ of motion at the innermost point of the sectors.

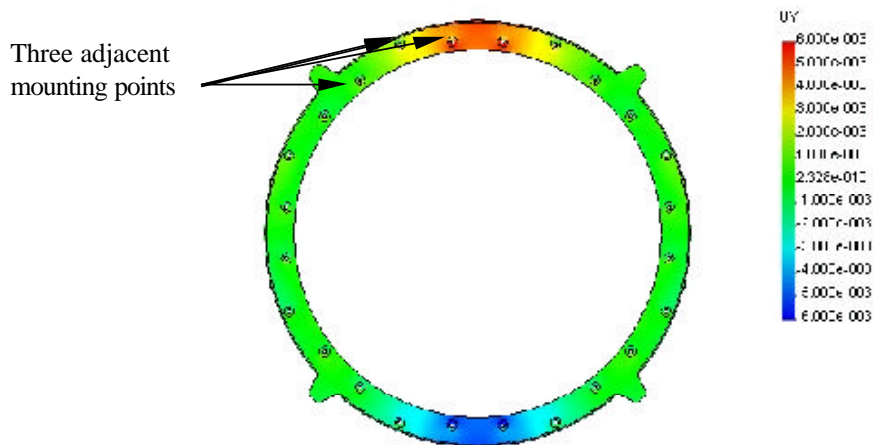


Figure 4: Ring (PEEK Inserts) contraction in the Ydirection for the 40°C uniform change in temperature. Units are mm.

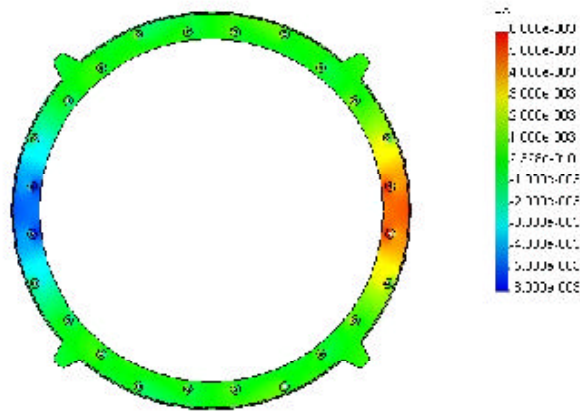


Figure 5: Ring (PEEK Inserts) contraction in X-direction for the 40°C uniform change in temperature. Units are mm.

The PEEK material for the inserts was replaced with the properties for 3D C-C and additional solutions were made. The contraction of the bushings is substantially reduced, as one would expect. The contraction at the mounting interface is predicted to be 0.38 μ m, Figure 6.

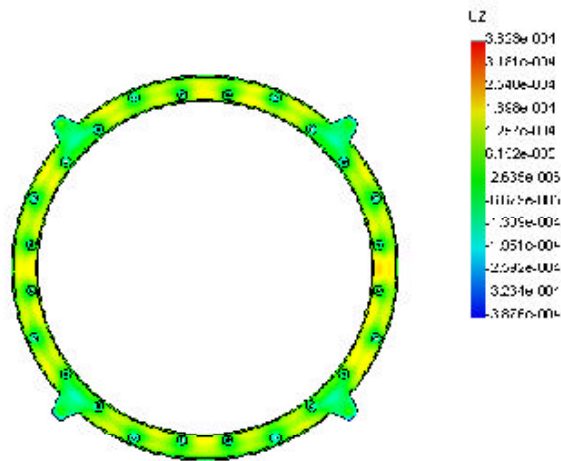


Figure 6: Ring (3D C-C inserts) out of plane distortion due to uniform temperature change from room to -15°C. Peak contraction at ring/sector interface is 0.38mm

Replacing the bushing inserts with 3D C-C material does not materially change the solution for static stiffness, as evidenced by the results of Figure 7. A slight increase in stiffness is observed, but hardly significant. In addition, the radial thermal strain likewise remains

unchanged (Figure 8). This distortion¹ is a direct result of the choice of the boundary conditions for the ring, i.e., the fixed radial restraint.

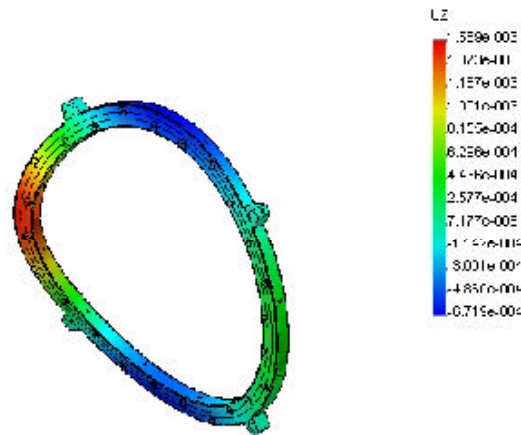


Figure 7: Displacement normal to ring (3D C-C inserts) cross-section due to 1N applied load. Load application uniformly applied over two bushings in center of ring arc. Displacement units are mm; maximum displacement is nominally 1.56mm.

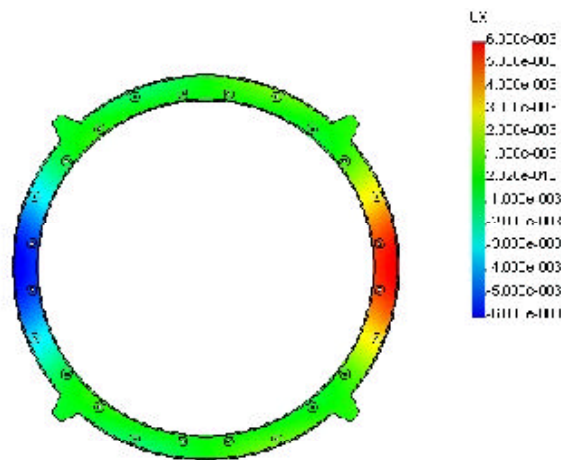


Figure 8: Predicted thermal strain in X-direction for composite support ring using 3D C-C bushing inserts for a temperature differential of -40°C. The peak radial movement is nominally 6mm.

Figure 9 depicts the distortion in the ring due to two radial loads exerted on the upper two mount locations. This loading condition is intended to provide a measure of the ring radial compliance. The two upper mounts were “free” in the radial direction only, i.e., the

¹ Mesh had to be regenerated between the two material candidates due to a loss of the FEM file. A slight difference exists in the total number of nodes and elements between the two material solutions. This may account for the slight difference between Figure 5 and Figure 8.

circumferential direction is fixed. The two lower mounts are fixed both radial, and tangentially. The radial compliance for the specified conditions is $0.123\mu\text{m}/\text{N}$, or possibility more conveniently $0.55/\mu\text{m}/\text{lbf}$.

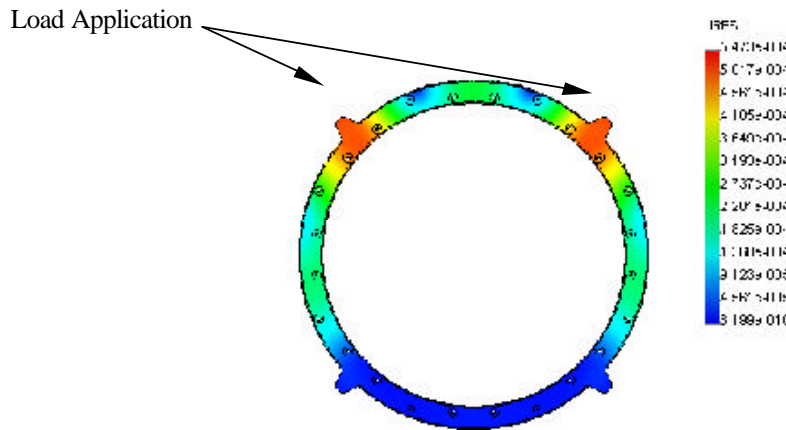


Figure 9: Resultant distortion in ring due to 4.448N loads applied radially at two upper mount positions. Two lower mount points are fixed. Peak radial deflection is 0.55mm (0.123mm/N or 0.55mm/lbf)

3. Conclusions

Although, the investigation of the ring behavior was somewhat limited in scope one may draw several tentative conclusions. The conclusions that followed are clouded by the lack of knowledge regarding the coupled behavior of the ring with the outer frame structure. Nonetheless, the following seems apparent:

- a. The CTE of the mounted ring structure is on the order of $-0.87\text{ppm}/^\circ\text{C}$. This number is derived by the X/Y distortions reported in Figure 4, Figure 5, and Figure 8. The nominal peak distortion is $6\mu\text{m}$ (ring diameter=345.24mm, 40°C).
- b. The particular orientation chosen for the sector-mounting pattern will tend to couple sector ϕ movement with changes in radial distortions, assuming the outer frame restrains the ring as modeled. Rotation of the sector comes from the off-center mounting of the sector relative to the radial planes of ring symmetry.
- c. The low radial compliance (high stiffness) of the ring to forces applied in an opposing sense makes it difficult to store elastic energy. A thought of storing an elastic deformation in the ring for mounting of the ring has been advanced; this objective was to be accomplished without resorting to spring loads in the mount design.
- d. The benefit of using C-C for the sector mounting bushings in the mounting ring is evident. The positional change that results from a 40°C is negligible.